OTC 18860

Numerical Studies of Geomechanical Stability of Hydrate-Bearing Sediments

Jonny Rutqvist and George J. Moridis, SPE, Lawrence Berkeley National Laboratory

Abstract

The thermal and mechanical loading of oceanic Hydrate-Bearing Sediments (HBS) can result in hydrate dissociation and a significant pressure increase, with potentially adverse consequences on the integrity and stability of the wellbore assembly, the HBS, and the bounding formations. The perception of HBS instability, coupled with insufficient knowledge of their geomechanical behavior and the absence of predictive capabilities, have resulted in a strategy of avoidance of HBS when locating offshore production platforms, and can impede the development of hydrate deposits as gas resources.

In this study we investigate in three cases of coupled hydraulic, thermodynamic and geomechanical behavior of oceanic hydrate-bearing sediments. The first involves hydrate heating as warm fluids from deeper conventional reservoirs ascend to the ocean floor through uninsulated pipes intersecting the HBS. The second case describes system response during gas production from a hydrate deposit, and the third involves mechanical loading caused by the weight of structures placed on the ocean floor overlying hydrate-bearing sediments.

For the analysis of the geomechanical stability of HBS, we developed and used a numerical model that integrates a commercial geomechanical code and a simulator describing the coupled processes of fluid flow, heat transport and thermodynamic behavior in the HBS. Our simulation results indicate that the stability of HBS in the vicinity of warm pipes may be significantly affected, especially if the sediments are unconsolidated and more compressible. Gas production from oceanic deposits may also affect the geomechanical stability of HBS under the conditions that are deemed desirable for production. Conversely, the increased pressure caused by the weight of structures on the ocean floor increases the stability of underlying hydrates.

Introduction

Background. Gas hydrates are solid crystalline compounds in which gas molecules (referred to as guests) are lodged within the lattices of ice crystals (called hosts). Under suitable conditions of low temperature and high pressure, a gas G will react with water to form hydrates according to

$$G + N_H H_2O = G \bullet N_H H_2O,$$

where N_H is the hydration number. Of particular interest are hydrates formed by hydrocarbon gases when G is an alkane. Natural hydrates in geological systems also include CO_2, H_2S and N_2 as guests. Vast amounts of hydrocarbons are trapped in hydrate deposits[1]. Such deposits occur in two distinctly different geologic settings where the necessary low temperatures and high pressures exist for their formation and stability: in the permafrost and in deep ocean sediments.

The three main methods of hydrate dissociation are[2]: (1) depressurization, in which the pressure P is lowered to a level lower than the hydration pressure P_e at the prevailing temperature T, (2) thermal stimulation, in which T is raised above the hydration temperature T_e at the prevailing P, and (3) the use of inhibitors (such as salts and alcohols), which causes a shift in the P_e-T_e equilibrium through competition with the hydrate for guest and host molecules. Dissociation of the solid hydrate phase results in the production of gas and water.

Gas hydrates exist in many configurations below the sea floor, including massive (thick solid zones), continuous layers, nodular, and disseminated, each of which may affect the seafloor stability differently. The hydrates in all of these configurations may be part of the solid skeleton of the load-bearing formation, which ultimately supports platforms and pipelines needed for production from conventional oil and gas resources, and from hydrate accumulations (when it becomes economically and technically viable).

The thermal and/or mechanical loading of Hydrate-Bearing Sediments (HBS) can result in hydrate dissociation and a significant pressure increase, with potentially adverse consequences on the integrity and stability of the wellbore assembly, the HBS, and the bounding formations. The perception of HBS instability, coupled with insufficient knowledge of its geomechanical behavior and the absence of predictive capabilities, has led to the avoidance of HBS when locating offshore production platforms, and can emerge as an impediment in the development of hydrate deposits as gas resources.

Objective and Problem Description. The main objective of this study is to evaluate the geomechanical stability of oceanic HBS subjected to thermal, mechanical and hydraulic loading. We investigate the behavior of oceanic HBS systems in three

cases that involve coupled (interacting) hydraulic, thermal, thermodynamic and geomechanical processes and phenomena.

The first case involves hydrate heating as warm fluids from deeper conventional reservoirs ascend to the ocean floor through uninsulated pipes intersecting the HBS. Note that, although geomechanical stresses occur in both permafrost and oceanic hydrate accumulations exposed to the aforementioned processes, the consequences and their severity differ substantially between the two types of hydrate deposits. Thus, the proximity of HBS to the ocean floor can have catastrophic economic and safety consequences in marine hydrate accumulations.

The second case addresses the question of system response during gas production from a hydrate deposit. Depressurization-based gas production from HBS leads to the gradual depletion of the hydrates, in addition to a pressure drop. Thus, the weight of the overlying sediments (initially borne by a composite solid phase comprising the grains of the porous medium and the cementing hydrates) is carried by a progressively smaller solid volume as hydrates dissociate, while the counteracting fluid pressure declines. Depending on the properties of the porous medium, this can lead to significant geomechanical changes (including compaction and subsidence), in addition to potentially important impacts on the hydraulic properties of the geologic media. These geomechanical and hydraulic changes can affect further gas production and the integrity of the wellbore assembly.

The third case involves mechanical loading caused by the weight of structures placed on HBS at the ocean floor, and the effect on HBS stability of mechanical stresses caused by the weight and the anchoring of offshore platform structures and pipelines within the hydrate deposits. The hypothesis to be tested is whether the resulting higher pressures can cause partial hydrate dissociation at the locations of maximum stress (in a manner akin to ice melting at higher pressures) and, if these are extensive, the loss of stability, and the potential for submarine landslides when such structures are located on slopes.

Geomechanical properties of the HBS

Because of the paucity of data on the geomechanical behavior and properties of HBS, we apply mechanical properties representing different host sediments ranging from soft unconsolidated clays to competent sandstones. To simulate the mechanical behavior of the HBS, we apply an elastoplastic mechanical model, with a modified Mohr-Coulomb failure criterion. The elastic-plastic properties of the HBS are dependent on the properties of the host medium (e.g. sandstone or clay), which are modified to take into account the cementing effects of pore-filling hydrates.

Table 1 lists the properties of the three types of porous media in HBS considered in this study: Toyoura sand[3], clay, and a competent sandstone (such as the Berea Sandstone). In the base case of this study, the geomechanical properties of the HBS were taken from the laboratory experiments of *Masui et al.*[3] on hydrate-bearing Toyoura sand. The parameters describing the mechanical properties of the Toyoura sediment are corrected for pore-filling solid content (hydrate and ice). Following the approach of *Masui et al.*[3], we assumed that certain mechanical properties (bulk and shear moduli, and cohesion) increase linearly with hydrate saturation. Such an assumption is necessitated by the dearth of laboratory or field data on the subject. For example, the cohesion varies from 0.5 MPa at 0% hydrate saturation to an extrapolated 2.0 MPa at 100% hydrate saturation (Table 1). This linear model matches the laboratory data quite well over the range of hydrate content relevant to this study. Additionally, following the experimental results of *Masui et al.*[3], the friction angle is considered independent of the hydrate saturation S_H and equal to 30°.

Among the properties listed in Table 1, only the properties for Toyoura sand were rigorously determined from laboratory experiments on HBS. The properties of the unconsolidated soft clay in Table 1 represent reasonable approximations that were either inferred from typical values for clay, or were extrapolated from laboratory data[3]. Thus, the properties of soft clay (i.e., the cohesion and the bulk and shear moduli) were approximated as being 25% of the corresponding Toyoura sand values. Because the competent Berea Sandstone is comparatively stiff and cohesive, we assumed that the pore-filling solid content (hydrate and ice) had a minimal effect on the HBS's mechanical properties in that case.

Note that the base case in our geomechanical studies involves the Toyoura sand properties, and is the most internally consistent with the hydraulic and thermal properties used in the multi-phase flow and heat transport calculations. The studies based on the mechanical properties of clay and Berea sandstone are conducted for the comparative evaluation of the relative geomechanical responses of the various geological media in HBS.

The numerical simulation code

For the analysis of the geomechanical stability of HBS, we developed and applied a numerical model that integrates a commercial geomechanical code into a simulator describing the coupled processes of fluid flow, heat transport and thermodynamic behavior in geologic media. The starting point of our approach is the TOUGH+HYDRATE simulator[4-6], which describes the system hydraulic, thermal, and thermodynamic behavior in geological media containing gas hydrates. This code predicts the evolution of all the important thermophysical properties (e.g., pressure, temperature, phase saturation distribution, salt concentration, etc.) in hydrate-bearing systems undergoing changes through any combination of mechanisms that can induce hydrate dissociation or formation[2], i.e., changes in pressure, temperature, and/or in the concentration of inhibitors (such as salts and alcohols). To consider geomechanical effects, the TOUGH+HYDRATE code was coupled with FLAC3D[7] geomechanical simulator. This simulator is widely used in soil and rock mechanics engineering, and for scientific research in academia. FLAC3D has built-in constitutive mechanical models suitable for soil and rocks, including various elastoplastic models for quasi-static yield and failure analysis, and viscoplastic models for time dependent (creep) analysis, that could be used directly or modified for analysis of geomechanical behavior of HBS.

In the resulting coupled simulator (hereafter referred to as T+F), the two constituent codes—TOUGH+HYDRATE and FLAC3D—are linked through a coupled thermal-hydrological-mechanical (THM) model of the HBS (Figure 1). The THM model is consistent with the porous media model (one of the several available as options in TOUGH+HYDRATE) that

describes media deformation as a result of geomechanical changes. The basic couplings between hydrological and mechanical processes in the deformable porous media are considered through:

(1) An effective stress law, that defines how a change in pore pressure affects mechanical deformation and stress, and
(2) A pore-volume model that defines how a change in stress or strain affects the fluid flow.

In addition, there are numerous couplings—including changes in mechanical and hydrological properties—that are consequences of changes in effective stress and pore-volume. The relationship between hydraulic and geomechanical properties is further complicated by couplings related to temperature changes, and the possible effects of inhibitors (salts are present in all oceanic hydrate deposits, and salts and alcohols are occasionally used to enhance hydrate dissociation). These coupling routines were developed within the framework of the object-oriented FORTRAN 95 architecture of TOUGH+[6] and the FISH programming language available in FLAC3D[7].

Note that, while all these interactions are accounted for in T+F using generally accepted models, information on the specific parameters describing the HBS behavior is currently scarce[8] because this area of research has so far received scant attention. Specialized laboratory experiments are needed to (a) validate and verify the mathematical models, and (b) to determine the corresponding parameters.

In Figure 1, the data exchanges between TOUGH+ HYDRATE and FLAC3D are illustrated with arrows going through the central THM model. The arrow on the right hand side of Figure 1 shows the transmission of the effective stress σ' and strain ε (that are computed in FLAC3D) to TOUGH+ HYDRATE for the calculation of the updated porosity ϕ, and of the corresponding porosity change $\Delta\phi$. This mechanically induced $\Delta\phi$ has an immediate effect on the fluid flow behavior. For example, if a change in σ' and ε causes ϕ to decrease, the pore pressure is expected to rise, especially if the permeability is low. Two models for mechanically induced porosity changes are implemented in the current version of T+F:

(1) A poroelastic model (based on the approach proposed by *Settari and Mourits*[9]) that considers macroscopic stress/strain changes and grain deformability, and
(2) An empirical model (proposed by *Rutqvist and Tsang*[10]) that describes a non-linear change in porosity as a function of the effective mean stress

The $\Delta\phi$ computed from either of these models is used to estimate changes in k by means of empirical equations[6,11]. The updated ϕ and k values are in turn used to estimate changes in the hydraulic and wettability properties of the porous medium (i.e., aqueous and gas phase relative permeabilities k_{rA} and k_{rG}, and capillary pressure P_c) by employing appropriate scaling equations[6,12] that are available as options in T+F.

The arrow on the left side of Figure 1 depicts the flow of data obtained from TOUGH+HYDRATE (namely the pressure P, temperature T, and phase saturations S_β) to FLAC3D for processing and estimation of their impact on the effective stress $\alpha\Delta P$ (α being Biot's effective stress parameter), as well as on the thermal and swelling strains (ε_θ and ε_{sw}, respectively) Additionally, changes in P, T and S_β result in changes in other HBS mechanical properties that are listed in Figure 1. These include the bulk modulus K, the shear modulus G, the cohesion C_m, and the coefficient of internal friction μ. The T+F model includes an empirical relationship to adjust the HBS geomechanical properties for changes in the solid phase saturations, i.e., hydrate and ice saturations (S_H and S_I, respectively). T+F allows the implementation of alternative models as more laboratory data and theoretical models relating S_H and S_I to mechanical properties become available.

The earlier work of *Rutqvist et al.*[13] (involving joint thermal, flow and geomechanical processes) incorporated a loosely coupled scheme, which involved interacting (rather than fully coupled) flow and geomechanical component codes, and was used to analyze coupled THM problems related to nuclear waste disposal and CO_2 geological sequestration. In the current T+F model, the two component codes TOUGH+ HYDRATE and FLAC3D are seamlessly integrated. FLAC3D is treated as a simple C-language subroutine that is invoked from within the FORTRAN 95 body of TOUGH+HYDRATE, resulting in a tighter and more rigorous coupling, and to substantially improved efficiency.

Three coupling schemes are available in T+F:

(a) *Jacobian*: This is the highest level of iterative coupling, in which all the geomechanical and flow parameters are continuously updated (in every Newtonian iteration of every timestep), and their changes are accounted for in the computation of the Jacobian matrix.
(b) *Iterative*: In this scheme, the geomechanical and flow parameters are corrected at the end of each Newtonian iteration of each timestep, and the contribution of their changes between Newtonian iterations are not accounted for in the computation of the Jacobian matrix.
(c) *Time-step*: This represents the weakest coupling option, and involves correction of the geomechanical and flow parameters once in (at the end of) each time step. As in the iterative scheme, the parameter changes do not contribute to the computation of the Jacobian matrix.

The full Jacobian option is a *sequentially implicit* scheme, whereas the iterative and the time-step coupling options are *sequentially explicit* schemes. The full Jacobian scheme is necessary in problems where pore-volume (direct) couplings dominate, i.e., when a mechanically induced $\Delta\phi$ gives rise to a relatively strong and rapid change in pore pressure, and where it is necessary to rigorously preserve the fluid mass and heat balances. In problems where the so-called property changes (indirect) couplings dominate, iterative or time-step coupling schemes are sufficient.

In this study we focus on the geomechanical behavior of the HBS, and we limit our simulations to one-way coupled analysis. That is, we investigate the effects that changes in P, T and S_β induce on the geomechanical stability of HBS (as described by all relevant geomechanical parameters), but we do not account for the effect of the mechanically induced changes in the hydraulic and wettability properties on the multiphase flow behavior. Such complete (two-way) coupling is the subject of a study currently in progress, and is far more

computationally intensive than the (already demanding) one-way coupling work discussed in this paper.

Problem 1: Hydrate heating through uninsulated pipes intersecting an oceanic HBS

Objective and problem description. The main objective of this problem is to investigate the response of marine HBS to thermal loading. Such thermal loading occurs when heat from hot reservoir fluids (produced from deeper reservoirs) flows into the HBS through uninsulated piping. This problem was first studied by *Moridis and Kowalsky*[14] using a code that did not have full geomechanical capabilities, but was limited to a simplified model of pore compressibility. As such, it could not internally estimate the σ and ε resulting from the P, T and S_β changes in response to the HBS heating and hydrate dissociation, and their subsequent effects on the HBS hydraulic, thermal and geomechanical properties system, and on the overall system behavior (e.g., deformation and subsidence). Thus, the analysis was limited to the prediction of the evolution of important hydraulic and thermal properties and conditions, which could then serve as inputs in subsequent geomechanical studies.

With the availability of the geomechanical capabilities of T+F, Problem 1 is revisited in order to investigate in detail the geomechanical stability of a complex HBS system under thermal loading. Because of the very large computational requirements of the geomechanical analysis, we concentrated on the reference case (Case A) of the *Moridis and Kowalsky*[14] study, and conducted a sensitivity analysis of the system response to changes in the geomechanical properties.

Rising temperature T in the HBS can have serious consequences[14]. Even before dissociation is attained, it is expected to affect the mechanical strength of hydrate-bearing sediments – possibly severely, given the narrow temperature difference between hydrate stability and dissociation. When T reaches the hydrate equilibrium temperature T_e (see Figure 2) at the prevailing pressure P (usually close to the hydrostatic pressure at the location), hydrate dissociation occurs. This leads to the rapid release of large amounts of gas, which can in turn result in rising pressure and, potentially, in formation fracturing. The consequences could be serious if the confining (impermeable) top boundary of an underlying reservoir is compromised and reservoir fluids escape. The increased P, if sufficiently high, could also have a detrimental effect on the wellbore assembly, including cement fracturing and wellbore collapse.

Another problem that might arise from thermal loading is the deterioration of the structural stability of the geologic formation in the vicinity of the wellbore. Hydrates are very effective cementing agents[8], and their dissociation can lead to substantial subsidence and other adverse geomechanical changes in the thermally affected region. Unless accounted for, these changes can pose a hazard to the structural stability of the wellbore assembly.

The reason for the concern is demonstrated in the photograph of Figure 3, which shows a dissociating core of a marine HBS. While the more isolated inner portion of the core (where hydrate still remains) appears "solid" and structurally strong, the medium in the outer annular space (where hydrate dissociation is in progress or has already occurred) has a fluid and very weak consistency because of the loss of the cementing hydrate and shows evidence of escaping gases (bubbling). Because of its consistency, the remaining watery mud is characterized as *soupy sediment*. The impact of its evolution on the structural stability of marine HBS demands evaluation, especially where compressible sediments such as marine muds and clays are involved. Finally, during dissociation, the basal zone of the gas hydrate can become under-consolidated and possibly over-pressurized because of the newly released gas[15], leading to a zone of weakness (characterized by low shear strength, where failure could be triggered by gravitational loading or seismic disturbances) and the possibility of submarine landslides[16,17].

Geology and model setup. The geometry and HBS multiphase fluid and heat transport properties are as described by *Moridis and Kowalsky*[14], and represent realistic geology and conditions found in natural oceanic HBS (Figure 4). The geology composed of a layered sequence of five formations (A through E), confined at the top and bottom by effectively impermeable shale layers (designated as formations U and L, respectively). The most important hydrologic and thermal properties and parameters of the various formations involved in hydrate dissociation, multiphase flow and heat transport are given in Tables 2 and 3.

The geomechanical properties are listed in Table 1. As discussed above, the base case involved the geomechanical properties of the Toyoura sand[3], while the properties of an unconsolidated clay were also used for sensitivity analysis studies. All five hydrate-bearing formations, as well as the overburden to the surface and the underburden, were assumed to have the same geomechanical properties.

In this simulation, heat from the hot fluids in the inner tubing flows through the well assembly to the hydrate-bearing formations, causing a temperature rise and hydrate dissociation. The confining formations, although impermeable, allow heat exchange with the overburden and the underburden. The gas released from dissociation cannot, therefore, escape into the ocean, but remains trapped and leads to higher pressures. The geothermal gradient to the base of the hydrate (i.e., at the bottom of layer E) was dT/dz = 0.0332 ^{o}C/m. With this geothermal gradient, the base of the hydrate layer coincided with the bottom of the hydrate stability zone, at which elevation P = 12.4 MPa.

Model domain and boundary conditions. As before[14], an infinite-acting single-well system was used. The outer reservoir radius was placed at r_{max} = 1000 m, where an outer constant-conditions boundary was located. However, in the present coupled multiphase fluid flow and geomechanical simulation, a 3-D grid (representing one quarter of the single-well system) was adopted (Figure 4a) instead of the 2-D cylindrical domain of *Moridis and Kowalsky*[14]. This was necessitated by the grid requirements of FLAC3D, and allowed the application of appropriate geomechanical boundary conditions and consideration of anisotropic *in situ* stresses. The domain was discretized into 30,000 gridblocks, resulting in 120,000 simultaneous equations. The uppermost and lowermost layers were constant temperature, no-flow boundaries, while the layers corresponding to the top and bottom confining layers (overburden and underburden, respectively, i.e., formations U and

L, Table 3) were impermeable but allowed heat exchange with the adjacent hydrate layers.

The design and material properties of the wellbore assembly, along with details of the system geometry, are given in Table 4 and in Figure 4b. In the discretized domain, the first 23 radial elements (Figure 4b) describe the well system, and provides a high-resolution description of the heat flow into the HBS through the inner tubing, the five steel casings (including the outer conductor), and the corresponding cement– and brine–filled annular spaces.

In terms of geomechanical boundary conditions, (a) the uppermost boundary was allowed to move freely, (b) the lowermost boundary was fixed for normal displacements, whereas (c) the horizontal outer boundary (i.e., at $r = r_{max}$) was fixed for any displacement. Additionally, a vertical stress representing the weight of the overlying water column was applied on the free moving top boundary.

Because previous studies[18,19,20] have shown that the most important processes and phenomena occur within a limited radius around the well, we also used a fine radial discretization in the HBS to describe accurately the critically important vicinity of the wellbore (especially in the $r < 25$ m zone). The thermal properties of the different components of the well assembly can be found in Table 4.

In terms of mechanical behavior, the well was simulated as a rigid boundary with the displacement normal to its surface fixed to zero. Such a rigid mechanical boundary is justified because oceanic sediments (here represented by Toyoura sand and clay) are much softer than the materials (steel and cement) in the well assembly. In principal, the well assembly could also be included explicitly in the mechanical calculation for a more detailed investigation of its mechanical response to the HBS dissociation.

Initial conditions. We determined the initial conditions in the reservoir by following the initialization process described by *Moridis and Kowalsky*[14]. The initial temperature distribution was computed from the known temperature at the mud line (5 ^{o}C at the upper boundary of the model) and the corresponding geothermal gradients. The pressures in the subsurface profile were assumed to follow a hydrostatic distribution. This is consistent with observations of natural hydrate accumulations in geologic media[21]. The initial pressures were computed using the water depths reported earlier, and a pressure-adjusted saline water density typical of ocean water (1030 kg/m^3 at atmospheric pressure). In this first simulation of coupled geomechanical system response, we assumed an isotropic initial stress field that increases with depth below the ocean floor and is based on a geologic medium bulk density of 2600 kg/m^3.

Simulation steps and outputs. The simulation period was 30 years, corresponding to the typical production life span of the deeper hot reservoir. In this first attempt to model complex and coupled multiphase fluid flow, heat transport and geomechanical interactions, we begin with a one-way coupled analysis focusing on the mechanical stability of the HBS. The results of the multiphase flow and heat transport part are essentially the same as those earlier reported[14]. This was expected because the systems were identical in all aspects except the grid geometry.

Thus, as a result of heat exchange between the hot production fluids and the colder (initially) hydrate-bearing formation, T in the HBS increases, hydrate dissociation begins, gas and water are released, and the pressure rises. Dissociation tends to be self-limiting because it is strongly endothermic (thus consuming a large portion of the heat supplied by the wellbore), and because the rising pressure makes further dissociation progressively more difficult. Details of the spatial evolution and distribution of pressure, temperature, hydrate, gas, and aqueous saturations, as well as salinity, over the 30-year period are given in *Moridis and Kowalsky*[14]. Here, we will focus only on the distribution of parameters relevant to the geomechanical behavior of the HBS.

Spatial distributions of key variables. Figures 5a to 5c show evolution of P, T and S_H. In Figure 5a, the P distribution indicates that the region of maximum pressure P_{max} is observed in the lowermost hydrate-bearing formations (where the lowest k and ϕ, and the highest S_H occur). The T distribution in Figure 5b indicates that the temperature rise caused by the heating from the wellbore affects mostly a narrow cylindrical zone. The hydrate saturation distribution in Figure 5c is limited in extent, decreases with depth, and is barely larger than $r = 15$ m at its maximum after 30 years of heating. The *staircase* appearance of S_H distributions in Figure 5c is attributed to the layered pattern (Table 3) of decreasing k and increasing S_H with depth[14]. In Figure 5a we observe a very significant pressure rise at the bottom of formation E, which is expected to induce significant geomechanical responses.

Geomechanical stress and failure. Figure 6 presents the evolution over time of key principal stress σ components. Figure 7 shows the evolution of volumetric strain ε_v. In Figure 7, the red contour area of large volumetric strain is a good indicator of *yielding*, which occurs when the critical stress (as defined by the Mohr-Coulomb criterion) is exceeded and leads to inelastic deformation.

In general, the yield zone (indicated by the region of large volumetric strain ε_v) in Figure 7 coincides with the zone of near-zero minimum compressive effective stress σ'_{min} in Figure 6b. A near-zero effective stress indicates that the increased fluid pressure caused a complete unloading and tensile failure. This near-zero σ'_{min} in Figure 6b is oriented vertically—indicating that horizontal tensile fractures could form—and is especially evident near at the bottom of layer E of the HBS, i.e., at its interface with the lower impermeable formation L. Note that tensile failure may be accompanied by shear failure caused by high shear stress.

The relatively high ε_v in the upper part of the system (Figure 7) is not necessarily coincident with the zone of near-zero σ'_{min}, but may be in part the result of the lower S_H at that location. The cohesion C_m of the HBS is proportional to S_H in Figure 5c. Thus, $C_m = 0.5$ MPa in an HBS layer that has experienced complete hydrate dissociation (indicated by the purple contour in Figure 5c), and increases linearly with S_H (see Table 1) in the undisturbed parts of the lowermost hydrate layer E (where the highest S_H occurs). Figure 7 indicates (a) the potential for collapse of the HBS in the vicinity of the well assembly, and (b) that the failure zone could propagate (mov-

ing upward through the sediments from layer E toward layer A) to reach the upper impermeable layer after 20 to 30 years.

Figure 6a shows that high compressive stress develops at the well assembly near the bottom of the layered HBS, where the fluid pressurization is at its highest (Figure 5a). The corresponding higher total compressive stress is caused by the increasing fluid pressure in the geomechanically-constrained medium. The highest compressive stress is oriented along the radial direction, which means that this stress acts upon the well assembly. However, adverse consequences are not expected because of the steel and cement involved in the construction of the well assembly are mechanically competent.

Effect of geomechanical properties on the system response. To determine the effect of the texture of the geologic media on the geomechanical response of the system in Problem 1, we conducted an additional coupled geomechanical simulation assuming the properties of an unconsolidated clay (applied to all layers) in addition to the reference case involving Toyoura sand[3] (Table 1). The hydraulic and thermal properties were retained as in the base case (Table 3) to ensure a comparison limited to the effects of geomechanical properties.

Figure 8 compares the volumetric strain and vertical displacement for the two different media textures. The extent and magnitude of volumetric strain is significantly larger for the softer clay, especially near the top and bottom impermeable layers. The vertical displacement is also larger. Settlement (subsidence) of up to 1 m is observed near the lower impermeable layer. Conversely, a small uplift on the order of 0.1 to 0.2 m is observed at the ocean floor. This uplift is caused by the increased fluid pressure in the upper HBS layers, where the gas released from hydrate dissociation accumulates because the impermeable overburden prevents escape.

Problem 2: Geomechanical system response during gas production from an oceanic Class 3 deposit

Problem description. The main objective of this problem is to investigate whether geomechanical changes during gas production from an HBS undergoing depressurization-induced dissociation can adversely affect the stability of the system and further production. The concern is that the progressive transfer of mechanical loads from the solid hydrate to the geologic media (as hydrate dissociates) can have a negative impact on the wellbore stability and structural integrity. Reductions in the media ϕ and k, (and, consequently, changes in $k_{r\beta}$ and P_c), with corresponding adverse consequences for gas production, are also possible. Additionally, subsidence has to be investigated to address its impact on structures anchored to the ocean floor.

System geology, properties, and initial conditions. The geologic system in this study was based on that of the Tigershark area[22] located in the Alaminos Canyon Block 818 of the Gulf of Mexico. Log data from an exploration well in about 2750 m (9000 ft) of water at the site indicated the presence of an 18.25-m (60-ft) thick sandy HBL (10,530 to 10,590 ft drilling depth) with a porosity ϕ of about 0.30 and Darcy-range intrinsic permeability[22]. Preliminary calculations[18] indicate that the S_H is in the 0.6-0.8 range, and that the base of the gas hydrate stability zone at this location occurs at or slightly below the base of the HBL[22,23].

The hydrate accumulation in Problem 2 is assumed to be a Class 3 deposit[20], i.e., composed of a single hydrate interval and bounded by confining (impermeable) layers, with no underlying zone of mobile fluids. Although the Tigershark deposit is a Class 2 deposit[19] (i.e., with a zone of mobile water underlying the hydrate layer), its properties are particularly valuable in the study of a Class 3 deposit because they describe a promising target for gas production (as indicated by the high S_H and the thermodynamic proximity of the HBL to the Lw-H-V line in Figure 2), and because there are few other such data available. The initial conditions, and the most relevant multi-phase flow and heat transport properties are provided in Table 5.

Production approach and model setup. Gas production from this Class 3 deposit was investigated by *Moridis and Reagan*[20], who employed constant-pressure production using vertical wells. In this study, we investigate depressurization-induced gas production from the same hydrate deposit using a horizontal well maintained at a constant pressure. This type of production method is recommended in Class 3 deposits[20] because of uncertainties over (a) the magnitude of the effective permeability k_{eff} of the original (undisturbed) HBS, and (b) the k_{eff} evolution over time. These uncertainties preclude constant-rate production.

Production in Problem 2 involves a system of parallel horizontal wells, with a well spacing of 1,000 m. Within the HBS, the horizontal well is located 1 m below the impermeable ovrburden. Hydrate is depressurized by applying a constant pressure P_w = 2.8 MPa at the well. Because of the symmetry of the well configuration and of the production approach, only a fraction of the affected domain need be modeled. Figure 9 shows the configuration of the parallel well system (upper part), and the geometry of the simulated domain (lower part), which represents a unit length (= 1 m) of the horizontal well. The domain is discretized in 97 x 106 = cells in (x,z), resulting in about 10,300 cells and about 50,000 simultaneous equations.

We investigated the geomechanical behavior of the HBL in the course of depressurization-induced gas production using the mechanical properties of all three types of the host media listed in Table 1 (i.e., the base case of the Toyoura sand[3], an unconsolidated clay, and the Berea competent consolidated (lithified) sandstone). In all cases, the impermeable confining layers were assumed to have the same geomechanical properties as the HBS they bound. For example, if the HBS is assumed to be composed of the weak Toyoura sand, then the surrounding impermeable layers are considered to be weak shales with the same geomechanical properties.

Simulation steps and outputs. The simulation period in this case is limited to 1 year, because this time was deemed sufficient long to observe significant pressure and temperature changes, in addition to substantial hydrate dissociation (with the corresponding phase changes) near the well. Because the HBS is hydraulically confined by shales, depressurization is expected to be rapid and effective, leading to hydrate dissociation and cooling (because of the strongly endothermic na-

ture of the hydrate reaction). The largest drop in pressure occurs in the vicinity of the well. The pressure differential induces flow of gas and water released from dissociation toward the well, and the flow is expected to increase over time (at least initially) as hydrate dissociation proceeds and k_{eff} increases.

In the multiphase flow component of the T+F simulation, we monitor the evolution of the rates of gas release, gas production and water production (Q_R, Q_P and Q_W, respectively), as well as the salt mass fraction X_P of the produced water (Figures 10 and 11). Additionally, we calculate the spatial evolution and distribution of the following flow-related variables: P, T, S_G, S_H, S_A, as well as the salt mass fraction X in the aqueous phase (Figures 12 and 13). These variables are the most relevant to the geomechanical behavior. The geomechanical variables that we determine as a result of changes in the conditions within the HBS in the course of gas production are discussed subsequently.

Production performance of the horizontal well. Before attempting to investigate the geomechanical response of the HBS to depressurization-based gas production, it is necessary to ascertain whether the use of a horizontal well is a viable approach, with its performance meeting some absolute and relative criteria of minimum performance[19,20] (the subject has not been investigated prior this study). Figure 10 shows the evolution of Q_R and Q_P during the first year of production for a 500 m-long horizontal well (production figures for different wells scale linearly).

The results in Figure 10 indicate that both gas release into the reservoir and production from horizontal wells are at their highest very early after the initiation of the operation (when the maximum pressure differential ΔP_w applies to the well). Q_R continues to decline monotonically during the entire production period, but Q_P stabilizes at about t = 55 days, and then rises slowly (as the effect of the decreasing ΔP_w on production is outweighed by the effect of a continuously expanding zone of increasing k_{eff} as dissociation advances). Finally Q_P begins a slow continuous decline (when a large HBS volume has dissociated, k_{eff} is either stabilized or increases very slowly, and the k_{eff} effect is overcome by that of the decreasing ΔP_w).

Figure 10 shows convincingly that the use of horizontal wells appears to be an attractive production option in Class 3 hydrate deposits, yielding large production rates Q_P (averaging 6.72 ST m^3/s = 20.5 MMSCFD for a 500 m-long well over the year-long production period of the study), and confirming earlier observations that Class 3 deposits appear to be promising gas resources[20]. Additional studies covering lengthier production periods are needed to determine the long-term performance of such wells.

The water production rate in Figure 11a indicates that Q_w is initially quite large (about 100 kg/s = 53,000 BPD on the first day), but declines rapidly, dropping to about Q_w = 30 kg/s (= 16,000 BPD) at t = 30 days, and to Q_w = 2.2 kg/s (= 1,160 BPD) at t = 360 days. These results are consistent with previous observations that the performance of hydrate deposits continuously improves with time in terms of water production[19,20]. Further confirmation of this continuous improvement is provided by the cumulative water-to-gas ratio R_{CWG} that is defined as

$$R_{CGW} = \frac{\int Q_w dt}{\int Q_p dt}$$

R_{CWG} provides a relative criterion, which, in addition to the absolute criteria of the magnitudes of Q_R and Q_P, is employed to evaluate the overall production performance of the system[19,20]. R_{CWG} in Figure 11b is shown to decline monotonically and exponentially with time, indicating continuous improvement of the water vs. gas balance. Thus, R_{CWG} reaches very low levels (4.89 kg of H_2O / ST m^3 of CH_4 = 0.84 Barrels of H_2O / MSCF of CH_4) in less than 10 days, and is further reduced to R_{CWG} = 2.27 kg of H_2O / ST m^3 of CH_4 = 0.39 Barrels of H_2O / MSCF of CH_4 at t = 360 days.

In Figure 1a, X_P drops rapidly, and is below 50% of its original value within a year from the inception of production. This was not unexpected, given that (a) there is no source of saline water other than that which coexisted initially with the hydrate in the pore space, and (b) hydrate dissociation releases large amounts of fresh water. The disposal of such low-salinity water (much lower than that of the water produced from vertical wells[20]) may be a cause for concern because it may adversely affect chemosynthetic communities if released near the ocean floor without mixing with ocean water at appropriate ratios.

Spatial distributions of key variables Figures 12a to 12d show the spatial distribution of P, T, and X in the domain, while Figures 13a and 13b show the corresponding distributions of S_H and S_G, respectively. The P distribution (Figure 12a) indicates a rather uniform depressurization of the reservoir, from initially 33 MPa, to about 3 MPa, as dictated by the constant pressure P_w = 2.7 MPa at the well. The cooling of the HBS (a direct consequence of the hydrate dissociation) is evidenced by the low temperature (from its original level of about 21 ^{o}C) in the formation (Figure 12b). As expected, the lowest temperature is observed near the well bore, where T drops to as low as 0.5 °C after 1 year of production (Figure 12b). This is because of the dissociation-induced general cooling, in addition to Joule-Thompson cooling as gas flows at high velocities near the wellbore.

The X distribution in Figure 12c indicates maximum salinity reduction at the top of the HBS (i.e., in contact with the impermeable overburden), and a significant salinity reduction at the base of the receding lower hydrate interface. The largest salinity reductions occur at the locations of maximum hydrate dissociation (Figure 13a), consistent with expectations[20]. Low-salinity water in contact with the impermeable boundaries may have significant implications for their geomechanical stability. Exposure of marine shales to fresh water can induce swelling and, consequently, structural weakening[14]. In this study we did not investigate the effects of fresh water release and swelling on the geomechanical performance of the shales confining the HBS.

Review of the phase saturations in Figure 13 indicates that the observations made in the study of gas production from Class 2 and Class 3 hydrates[19,20] using vertical wells apply to this problem of production from the Class 3 deposit using

horizontal wells. The depressurization-induced dissociation is characterized by the following common features:

(a) The evolution of an upper dissociation interface (Figure 13a) at the top of the hydrate layer (caused by heat flows from the upper boundary) that moves downward, in addition to the lower dissociation interface at the bottom of the HBL, which advances upwards as dissociation proceeds.
(b) Gas accumulation below the base of the overburden because of continuing dissociation and buoyancy-driven gas rise to the top of the formation (Figure 13b). The gas accumulation pattern has particularly important (and potentially severe) implications for gas production from oceanic deposits because lack of a confining overburden could lead to gas percolation though the overburden and release at the ocean floor.
(c) Processes and phenomena that occur within a narrow zone around the well control gas production from the entire hydrate deposit. The extent of this critical zone is limited to a few meters, and fine discretization must be used in its simulations if these near-well phenomena are to be captured and accurately described. Beyond the critical zone, dissociation, phase saturations and flow patterns are surprisingly uniform and have smooth gradients (Figures 12 and 13). This observation has important implications in the study of the geomechanical behavior of the HBS.

Geomechanical stress and failure analysis. The results depicted in Figures 14 through 16 are based on the mechanical properties of the Toyoura sand (Table 1), and describe the geomechanical response of the HBS at the end of the first year of production.

In Figure 14, the maximum compressive effective stress σ'_{max} is about 3 times the minimum compressive effective stress σ'_{min}. Note that the negative values in Figure 9 (and in the subsequent Figure 15) indicate compressive stress. The factor of 3 is dictated by the Mohr-Coulomb failure criterion, as computed for the 30° internal friction angle of the Toyoura sand. The results in Figure 14 indicate that the principal stresses are located on the Mohr-Coulomb failure envelope, and that continuous yielding (resulting in inelastic deformation) takes place after the Mohr-Coulomb criterion is attained.

The production (and the corresponding depressurization) tends to increase the shear stress in the reservoir, which is proportional to the difference between the maximum and minimum principal stresses. At the inception of production, the shear stress is zero because the initial stress field is isotropic. However, depressurization causes poroelastic stressing in the mechanically-confined horizontal direction, whereas the vertical stress remains constant because the model is free to contract in the vertical direction. This is illustrated in Figure 15, where the maximum compressive (vertical) principal stress σ_{max} remains constant and equal to its initial magnitude of -40 MPa. Conversely, the minimum compressive (horizontal) principal stress σ_{min} changes from its initial -40 MPa level to -12 MPa at the end of the first year of production.

In general, gas production and the associated depressurization increase the compressive effective stress in the reservoir, causing increased pressure on the grains of the HBS, which in turn increases shear strength.

Figure 16 shows the volumetric strain $\varepsilon_v = 0.44$, which is quite uniform in the HBS. Because of lateral confinement, the volumetric strain is equal to the vertical strain. The associated settlement at the top of the reservoir and at the ocean surface is $U_z = 0.8$ m. Most of this settlement (subsidence) is caused by elastic deformation during depressurization in the course of gas production, and the rest of the settlement is the result of yielding within the HBS. Because all of the subsidence occurs within the HBS, it important to consider it during the well design to avoid potential problems caused by shear stresses on the wellbore.

Review of the spatial distributions of the variables of interest in Figures 14 to 16 reveals a surprising uniformity of their magnitude in the entire HBS, as reflected by the lack of gradation in the corresponding contour plots. This observation is valid even in the immediate vicinity of the well (the critical zone), where localized variations in the multiphase flow variables are observed. The obvious conclusion is that the geomechanical response of the formation during gas production is uniform in the entire HBS, and this is attributed to the uniformity in the distribution of the multiphase flow variables discussed in the previous section. This uniformity may have important implications for the installation and anchoring of facilities on the ocean floor (including wellbore assemblies) over hydrate accumulations under production.

Effect of geomechanical properties on the system response. In addition to the base case discussed in the context of Figures 14 to 16, in Problem 2 we conducted two additional coupled simulations of geomechanical response of the HBS in the course of methane production using the geomechanical properties for an unconsolidated clay and of a Berea sandstone (Table 1). In these sensitivity analysis studies, the hydraulic and thermal properties of the base case (Table 5) were retained to ensure a comparison limited to the effects of geomechanical properties.

Table 6 presents the results of the comparison. The general geomechanical responses are similar (in terms of overall trend) for all three sets of mechanical properties, but they differ in magnitude. The largest fraction of settlement is essentially proportional to the deformation modulus of each medium, with the remainder depending on yielding. Although yielding occurs in the weaker Toyoura sand and clay, it is not observed in the competent Berea sandstone. The results of Table 6 indicate a higher σ_{min} in the weaker sediments. This is attributed to yielding, which tends to reduce the difference between maximum and minimum principal stresses. For example, in the case of the clay properties, the ratio of maximum to minimum compressive stress must be maintained below 2 in order to avoid exceeding the Mohr-Coulomb failure criterion (as computed for the 20° internal friction angle of the clay).

The potential for borehole stability was investigated by considering the theoretical elastic solution for stress concentrations around a borehole. In the cases of the Toyoura sand and of the clay, yielding is triggered at an early stage within the HBS, and consequently, the well bore is susceptible to yielding. With the Berea sandstone, the maximum tangential

stress occurs on the side of the horizontal borehole, and is calculated as $\sigma_\theta = 3\sigma_z - \sigma_x = 3 \times 40 - 9 = 111$ MPa. The tangential stress at the top and bottom of the borehole can be calculated as $\sigma_\theta = 3\sigma_x - \sigma_z = 3 \times 9 - 40 = -13$ MPa. These values substantially exceed the uniaxial compressive and tensile strengths for Berea sandstone. Hence, borehole instability is likely. The location of the horizontal well within the HBS may play a role in reducing this risk.

The calculated settlements U_z of 0.8 m and 4 m in the Toyoura sand and clay, respectively (Table 6), may adversely affect the integrity and stability of the wellbore assembly during gas production from dissociating hydrates in the HBS. If, on the other hand, the geomechanical properties of the reservoir medium are akin to the competent Berea sandstone, then settlement is expected to be insignificant (Table 6).

Problem 3: Loading caused by the weight of structures placed on hydrate bearing sediments at the ocean floor

Problem description. In this case we investigate the geomechanical behavior of oceanic HBS at or near the ocean floor, in which anchors or foundation of structures (such as offshore platforms) are installed. The host sediment is assumed to be weak and unconsolidated sediment with $S_H = 0.1$. Such a HBS is typical of a widely-occurring type of hydrate deposits[14,24] both in terms of texture (soft and structurally weak muds and clays are common at the ocean floor, with the cementing hydrates providing the only structural strength of the HBS) and hydrate saturation[25]. We load the system by applying a stiff-plate load under a static vertical load. The impact of the presence of hydrate was evaluated by comparing the results with and without the 10% initial hydrate saturation.

Stress and failure analysis. The preliminary analysis of this problem indicated that the thermodynamics of the system are sufficiently simple and straightforward that conclusions can be drawn without the need for a computationally demanding simulation. By increasing the load on the ocean floor (under the weight of a foundation or the tension of an anchoring cable), the effective compressive mean stress increases. Additionally, compression of the sediment can also result in a higher pore pressure as pores are mechanically squeezed. The magnitude of pressure increase depends on the load, whereas T remains almost constant (as it is controlled by the water T at the ocean floor, and its localized variations are short-term).

A simple review of the phase diagram in the hydrate P-T equilibrium graph of the water–CH_4–hydrate system in Figure 2 easily demonstrates why, unlike ice (that can melts under sufficiently high pressures), compression of the HBS cannot result in dissociation. At worst (in terms of thermodynamic and mechanical stability), hydrate in an HBS at the ocean floor can occur at a point along the 3-phase equilibrium line Lw–H–V. Increasing P at a constant temperature (a change depicted by the red arrow in Figure 2) moves the state of the system away from the hydrate-gas coexistence curve toward a more stable region of the phase diagram.

Thus, the hydrate becomes more stable, although S_H increases (albeit very slightly) because of the increased gas solubility in the aqueous phase. The analysis of this problem shows that the question of whether significant yielding of the HBS will occur is highly dependent on the mechanical properties (shear strength) of the host sediment. The presence of hydrate causes a strengthening of the HBS, hence indicating no adverse effects of hydrates for foundation.

Conclusions

In this study we investigated in three problems the coupled multiphase flow, thermal, thermodynamic and geomechanical behavior of oceanic HBS. The first involved hydrate heating as warm fluids from deeper conventional reservoirs ascend to the ocean floor through uninsulated pipes intersecting the hydrate bearing sediment. The second problem described system response during gas production (supported by depressurization-induced hydrate dissociation) from a Class 3 hydrate deposit, and the third involved mechanical loading caused by the weight of structures placed on an HBS. The analysis was conducted using the newly developed T+F numerical model that integrates geomechanical system analysis into a simulator describing the coupled processes of fluid flow, heat transport and thermodynamic behavior in geologic media.

Based on the results of this study, the following conclusions can be drawn:

(1) The stability of HBS in the vicinity of warm pipes may be significantly affected, especially near the ocean floor where the sediments are unconsolidated and more compressible. When geomechanically-weak sediments are involved, collapse of the formation around the wellbore is possible. Increasing geomechanical weakness of the host sediments adversely affects the system stability.

(2) Depressurization-based gas production from oceanic hydrate deposits may also significantly affect the geomechanical stability of HBS if structurally weak formations are involved. Stronger sediments exhibit little to negligible adverse geomechanical reaction to the results of depressurization and hydrate depletion during gas production. Conversely, geomechanically weak sediments such as clays can be severely affected. Consequently, care should be exercised during the design and installation of production structures and facilities on the ocean floor over HBS.

(3) The spatial distribution of all the geomechanical variables of interest is very uniform within the HBS because of the uniformity of the multiphase flow variables and conditions in the course of depressurization-induced gas production.

(4) The increased pressure caused by the weight of structures or anchoring stresses on the ocean floor increases the stability of hydrates.

It is important to point that these conclusions are valid only for the conditions and properties assumed in each of the problems we studied, and that extrapolations outside these limited regions are inadvisable because of the paucity of data on the subject and the limited body of relevant studies (insufficient to determine the envelope of possible system responses). However, the study clearly shows that the issue of geomechanical stability needs to be carefully analyzed at any field site involving HBS.

Nomenclature

C = specific heat (J/kg/K)
C_m = cohesion (Pa)
G = shear modulus of elasticity (Pa)
k = intrinsic permeability (m^2)
k_{eff} = effective permeability = $k\, k_{r\beta}$ (m^2)
$k_{r\beta}$ = relative permeability of phase β (= A, G, H)
k_Θ = thermal conductivity (W/m/K)
$k_{\Theta RD}$ = thermal conductivity of dry porous medium (W/m/K)
$k_{\Theta RW}$ = thermal conductivity of fully saturated porous medium (W/m/K)
K = bulk modulus of elasticity (Pa)
N_H = hydration number
P = pressure (Pa)
P_c = capillary pressure (Pa)
P_w = constant well pressure (Pa)
Q = volumetric rate (ST m^3/s)
Q_w = water mass production rate (kg/s)
R_{CWG} = cumulative water-to-gas ratio (kg/ST m^3)
x,r,z = coordinates (m)
r_{max} = maximum radius of the simulation domain (m)
S_β = saturation of phase β (= A, G, H)
t = time (days)
T = temperature (K or ^oC)
U_z = settlement, subsidence (m)
X = mass fraction of salt (kg/kg)

Greek Symbols

α = Biot's effective stress parameter (Pa^{-1})
α_P = Pore compressibility (Pa^{-1})
ε = strain
λ = van Genuchten exponent – Table 2
μ = coefficient of internal friction
σ = stress (Pa)
σ' = effective stress (Pa)
σ_θ = tangential stress (Pa)
ϕ = porosity
$\Delta\phi$ = porosity change

Subscripts and Superscripts

0 = denotes initial state
A = aqueous phase
B = base of HBS
e = equilibrium conditions
G = gas phase
H = solid hydrate phase
I = solid ice phase
irG = irreducible gas
irA = irreducible aqueous phase
max = maximum
min = minimum
n = permeability reduction exponent – Table 2
P = production stream
ref = reference Case C
R = rock, released
sw = swelling
v = volumetric
θ = thermal

Acknowledgment

This work was supported by the Assistant Secretary for Fossil Energy, Office of Natural Gas and Petroleum Technology, through the National Energy Technology Laboratory, under the U.S. Department of Energy, Contract No. DE-AC02-05CH11231. The authors are indebted to Matt Reagan for his assistance in the analysis and preparation of several plots, and for reviewing the manuscript. Thanks are extended to John Apps and Dan Hawkes for their careful review and helpful comments.

References

1. Sloan, E.D.: *Clathrate Hydrates of Natural Gases*, Marcel Dekker, Inc., New York, NY (1998).
2. Makogon, Y.F., *Hydrates of Hydrocarbons*. Penn Well Publishing Co. Tulsa, OK. (1997).
3. Masui, A., Haneda H., Ogata Y. and Aoki K. The effect of saturation degree of methane hydrate on the shear strength of synthetic methane hydrate sediments. Proceedings of the 5th International Conference on Gas Hydrates, Trondheim, Norway, 657–663 (2005).
4. Moridis, G.J., Numerical Studies of Gas Production From Methane Hydrates, *SPE Journal*, **32**(8), 359-370, (SPE paper 87330 - LBNL-49765) (2003).
5. Moridis, G.J., Numerical Studies of Gas Production from Class 2 and Class 3 Hydrate Accumulations at the Mallik Site, Mackenzie Delta, Canada, SPE Reservoir Evaluation and Engineering, **7**(3), 175-183, (2004).
6. Moridis, G.J. M. Kowalsky and K. Pruess, TOUGH-Fx/HYDRATE v1.0 User's Manual: A code for the Simulation of System Behavior in Hydrate-Bearing Geologic Media, LBNL number pending, 2005.
7. Itasca Consulting Group. Flac 3d, Fast Lagrangian analysis of continua in 3 dimensions, Minneapolis, Minnesota. (2002).
8. Durham, W.B., Kirby, S.H., Stern, L.A. and Zhang, W.: "The Strength and Rheology of Methane Clathrate Hydrate", *J. Geophys. Research*, **108**(B4), 2182 (2003).
9. Settari, A., and Mourits, F.M.: "A Coupled reservoir and Geomechanical Simulation System", *SPE Journal*, **27**(9), 219-226 (SPE paper 50939) (1998).
10. Rutqvist, J., and Tsang, C.F.: "Analysis of Thermal-Hydrologic-Mechanical Behavior Near an Emplacement Drift at Yucca Mountain", *J. Contaminant Hydrology*, **62–63**, 637–652 (2003).
11. Rutqvist, J., and Tsang, C.F.: "A study of Caprock Hydromechanical Changes Associated With CO_2 Injection Into a Brine Aquifer", *Environmental Geology*, **42**, 296-305 (2002).
12. Leverett, M.C.: "Capillary Behavior in Porous Solids", *Trans. Soc. Pet. Eng. AIME*, **142**, 152-169 (1941).
13. Rutqvist J., Wu, Y.-S., Tsang, C.-F., and Bodvarsson, G.: "A Modeling Approach for Analysis of Coupled Multiphase Fluid Flow, Heat Transfer, and Deformation in Fractured Porous Rock", *Int. J. Rock Mech. Min. Sci*. **39**, 429-442 (2002).
14. Moridis, G..J., and Kowalsky M.B.: "Response of Oceanic Hydrate-Bearing Sediments to Thermal Stress", OTC 18193, 2006 Offshore Technology Conference, Houston Texas, U.S.A., 1-4 May (2006).
15. Schmuck, E.A., and Paull, C.K.: "Evidence for Gas Accumulation Associated With Diapirism and Gas Hydrates at the Head of the Cape Fear Slide", *Geo-Marine Letters*, **13**,145 (1993).
16. McIver, R.D: Hydrates of natural gas–an important agent in geologic processes, in: *Abstracts with Programs*, 1089, Geological Society of America (1977).
17. Paull, C.K., Buelow, W.J., Ussler W., and Borowski, W.S.: "Increased Continental Margin Slumping Frequency During

Sea-Level Low Stands Above Gas Hydrate-Bearing Sediments, *Geology*, **24**, 143 (1996).
18. Moridis, G.J., Kowalsky, M.B., Pruess, K., "Depressurization-Induced Gas Production From Class 1 Hydrate Deposits," SPE 97266, 2005 SPE Annual Technical Conference and Exhibition, Dallas, Texas, U.S.A., October 9-12, 2005.
19. Moridis, G.J., and Reagan, M.T.: "Gas Production From Oceanic Class 2 Hydrate Accumulations", OTC 18866, 2007 Offshore Technology Conference, Houston, Texas, U.S.A., 30 April–3 May (2007).
20. Moridis, G.J., Reagan, M.T., "Strategies for Gas Production From Oceanic Class 3 Hydrate Accumulations," OTC 18865, 2007 Offshore Technology Conference, Houston, Texas, U.S.A., 30 April–3 May (2007).
21. Wright, J.F., Dallimore, S.R., and Nixon, F.M.: "Influences of Grain Size and Salinity on Pressure-Temperature Thresholds for Methane Hydrate Stability in JAPEX/JNOC/GSC Mallik 2L-38 Gas Hydrate Research-Well Sediments", in *Scientific Results from JAPEX/JNOC/GSC Mallik 2L-38 Gas hydrate research-well, Mackenzie Delta, Northwest Territories, Canada*. Dallimore, S.R., Uchida, T., and Collett, T.S., Eds., Geological Survey of Canada Bulletin 544, 229 (1999).
22. Smith, S., Boswell, R., Collett, T., Lee, M., Jones, E., "Alaminos Canyon Block 818: A Documented Example of Gas Hydrate Saturated Sand in the Gulf of Mexico," *Fire In The Ice*: NETL Methane Hydrates R&D Program Newsletter, 12 (Fall 2006).
23. Collett, T.S., Lee, M.W., *Well Log Analysis: Tiger Shark AC 818 No. 1*, U.S. Geological Survey, internal memo (2006).
24. Aoki, Y., Shimizu, S., Yamane, T., Tanaka, T., Nakayama, K., Hayashi, T., and Okuda, Y: "Methane Hydrate Accumulation Along the Western Nankai Trough", in *Gas Hydrates: Challenges for the Future*. Holder, G.D., and Bishnoi, P.R., Eds., Annals of the New York Academy of Sciences, **912**, 136 (2000).
25. Klauda JB, and Sandler, S.I.: "Global Distribution of Methane Hydrate in Ocean Sediment", *Energy & Fuels,* **19**, 469–478 (2005).
26. Moridis, G.J., Seol, Y., and T. Kneafsey: "Studies of Reaction Kinetics of Methane Hydrate Dissociation in Porous Media", Report LBNL-57298, Lawrence Berkeley National Laboratory, Berkeley, CA (2005).
27. van Genuchten, M.Th.: "A Closed-Form Equation for Predicting the Hydraulic Conductivity of Unsaturated Soils", Soil Sci. Soc., 44, 892 (19

Table 1 – HBS Geomechanical Properties

Property		Toyoura sand[a]	Clay[b]	Competent sandstone ("Berea")[c]
Cohesion C_m (MPa)	$S_H = 0$	0.5	0.125	21
	$S_H = 1$	2.0	0.5	21
Friction angle (°)	$S_H = 0$	30	20	35
	$S_H = 1$	30	20	35
Bulk Modulus K (MPa)	$S_H = 0$	95	24	28,000
	$S_H = 1$	670	670	28,000
Shear Modulus G (MPa)	$S_H = 0$	87	22	7,200
	$S_H = 1$	612	612	7,200

[a] **Fitted to experimental data in Masui et al.[3]**
[b] **Clay properties assumed to be 25% of Toyoura Sand**
[c] **From various literature sources**

Table 2 – Hydraulic and Thermal Properties in Problem 1[14]

Parameter	Value
Permeability k_r	10^{-15} m^2 (= 1 m D)
Porosity ϕ	0.30
Pore compressibility α_P	10^{-8} Pa^{-1}
Grain density ρ_R	2750 kg/m^3
Dry thermal conductivity $k_{\Theta RD}$	1.0 W/m/K
Wet thermal conductivity $k_{\Theta RW}$	3.3 W/m/K
Composite thermal conductivity model[26]	$k_{\Theta C} = k_{\Theta RD} + (S_A^{1/2}+S_H^{1/2})\ (k_{\Theta RW} - k_{\Theta RD}) + \phi S_I k_{\Theta I}$
Capillary pressure model[6,27]	$P_{cap} = -P_0 \left[\left(S^* \right)^{-1/\lambda} - 1 \right]^{-\lambda}$ $S^* = \frac{(S_A - S_{irA})}{(S_{mxA} - S_{irA})}$
S_{mxA}	1
λ	0.45
P_0	2000
Relative permeability model[6]	$k_{rA} = (S_A^*)^n$ $k_{rG} = (S_G^*)^n$ $S_A^* = (S_A - S_{irA})/(1 - S_{irA})$ $S_G^* = (S_G - S_{irG})/(1 - S_{irA})$ OPM model[6]
Relative permeability exponent[6] n	4
S_{irG}	0.02
S_{irA}	0.20

Table 3 – HBS layer properties in Problem 1[14]				
Formation	**Depth (m)**	**ϕ**	**k (mD)**	**S_H**
U	0–50	0	0	0
A	50–90	0.5	10^{-15}	0.20
B	90–130	0.475	10^{-16}	0.30
C	130–170	0.45	$5x10^{-17}$	0.40
D	170–210	0.425	10^{-17}	0.45
E	210–250	0.40	$5x10^{-18}$	0.50
L	250–280	0	0	0

Mbml: meters below mudline
Mudline elevation: -1000 m

Table 4 – Well design, description and properties[14]					
Component	**OD radius (in)**	**ID radius (in)**	**Density (kg/m^3)**	**k_Θ (W/m/K)**	**C (J/kg/K)**
Conductor	18	17	7850	45.35	461
Cement 1	17	10	1561	0.66	2100
Casing 1	10	9.365	7850	45.35	461
Cement 2	9.365	8	1561	0.66	2100
Casing 2	8	7.505	7850	45.35	461
Brine 1	7.505	6.6875	1250	0.55	4800
Casing 3	6.6875	6.2075	7850	45.35	461
Brine 2	6.2075	5.375	1250	0.55	4800
Casing 4	5.375	4.88	7850	45.35	461
Brine 3	4.88	2.75	1250	0.55	4800
Tubing	2.75	2.389	7850	45.35	461
Hot fluids	2.389	–	–	–	–

Table 5 – HBS Properties for Problem 2[20]	
Parameter	**Value**
Hydrate zone thickness	18.25 m
Initial pressure P_B (at base of HBL)	$3.3x10^7$ Pa
Initial temperature T_B (at base of HBL)	294.15 K
Gas composition	100% CH_4
Initial saturations in the HBL	$S_H = 0.7$, $S_A = 0.3$
Water salinity (mass fraction)	0.03
Initial saturations in the HBL	$S_H = 0.7$, $S_A = 0.3$
Intrinsic permeability $k_x=k_z$ (HBL and water zone)	$7.5x10^{-13}$ m^2 (= 0.75 D)
Intrinsic permeability $k_x=k_z$ (overburden & underburden)	0 m^2 (= 0 D)
Grain density ρ_R (all formations)	2750 kg/m^3
Constant pressure at the well P_w	$2.7x10^6$ Pa
Dry thermal conductivity $k_{\Theta RD}$ (all formations)	0.5 W/m/K
Wet thermal conductivity $k_{\Theta RW}$ (all formations)	3.1 W/m/K
Composite thermal conductivity model[26]	$k_{\Theta C} = k_{\Theta RD} + (S_A^{1/2}+S_H^{1/2})\ (k_{\Theta RW} - k_{\Theta RD}) + \phi\, S_I\, k_{\Theta I}$
Capillary pressure model[6,27]	$P_{cap} = -P_0\left[\left(S^*\right)^{-1/\lambda}-1\right]^{-\lambda}$ $S^* = \frac{(S_A - S_{irA})}{(S_{mxA} - S_{irA})}$
S_{irA}	1
λ	0.45
P_0	10^5 Pa
Relative permeability Model[6]	$k_{rA} = (S_A^*)^n$ $k_{rG} = (S_G^*)^n$ $S_A^*=(S_A-S_{irA})/(1-S_{irA})$ $S_G^*=(S_G-S_{irG})/(1-S_{irA})$ OPM model
n (from Moridis et al.[20])	3.572
S_{irG}	0.02
S_{irA}	0.25

Table 6 – Comparison of geomechanical behavior for different types of host sediments			
Parameter	Toyoura sand	Clay	Berea Sandstone
Minimum Compressive Reservoir Stress σ_{min} (MPa)	-12	-21	-9
Maximum Compressive Reservoir Stress σ_{max} (MPa)	-40	-40	-40
Magnitude of settlement of the ocean floor U_z (m)	0.8	4.3	0.05
Yielding within the HBS	Yes	Yes	No
Borehole instability	Yes	Yes	Yes

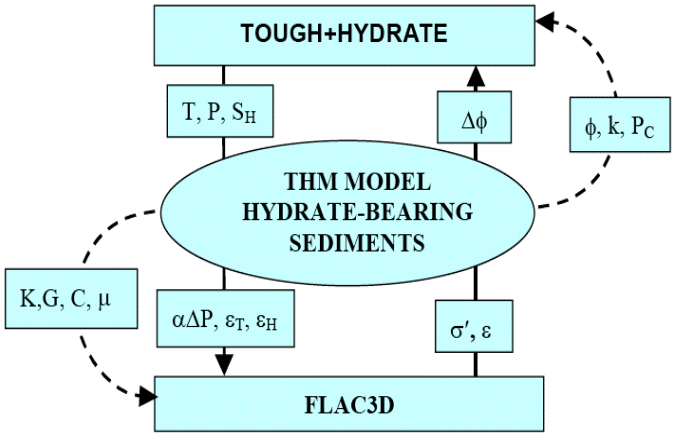

Figure 1 – Linking of TOUGH+HYDRATE with FLAC3D in the T+F code for the analysis of the geomechanical behavior of HBS.

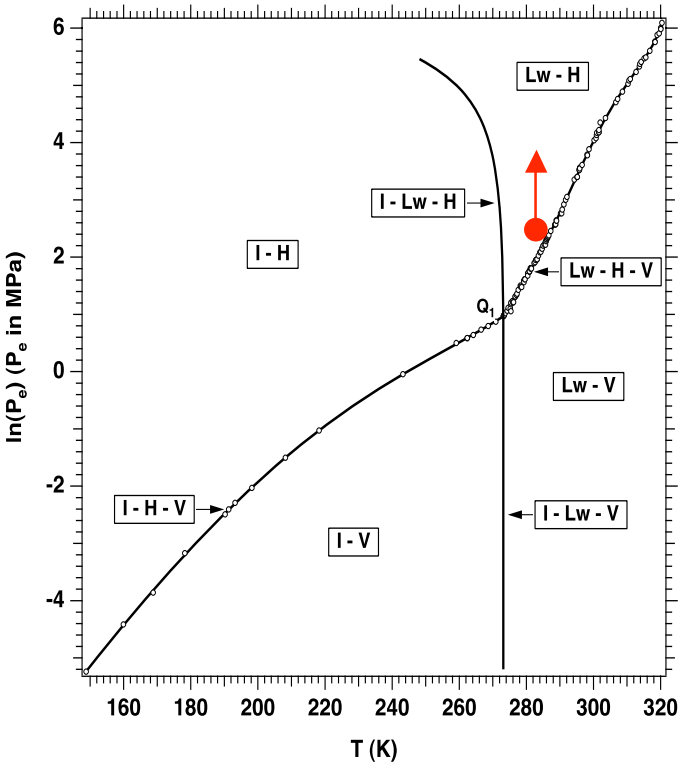

Figure 2 – Pressure-temperature equilibrium relationship in the phase diagram of the water–CH_4–hydrate system[12] (Lw: Liquid water; H: Hydrate; V: Vapor (gas phase); I: Ice; Q_1: Quadruple point = I + Lw + H + V) Pressure-temperature equilibrium relationship in the phase diagram of the water–CH_4–hydrate system[12] (Lw: Liquid water; H: Hydrate; V: Vapor (gas phase); I: Ice; Q_1: Quadruple point = I + Lw + H + V).

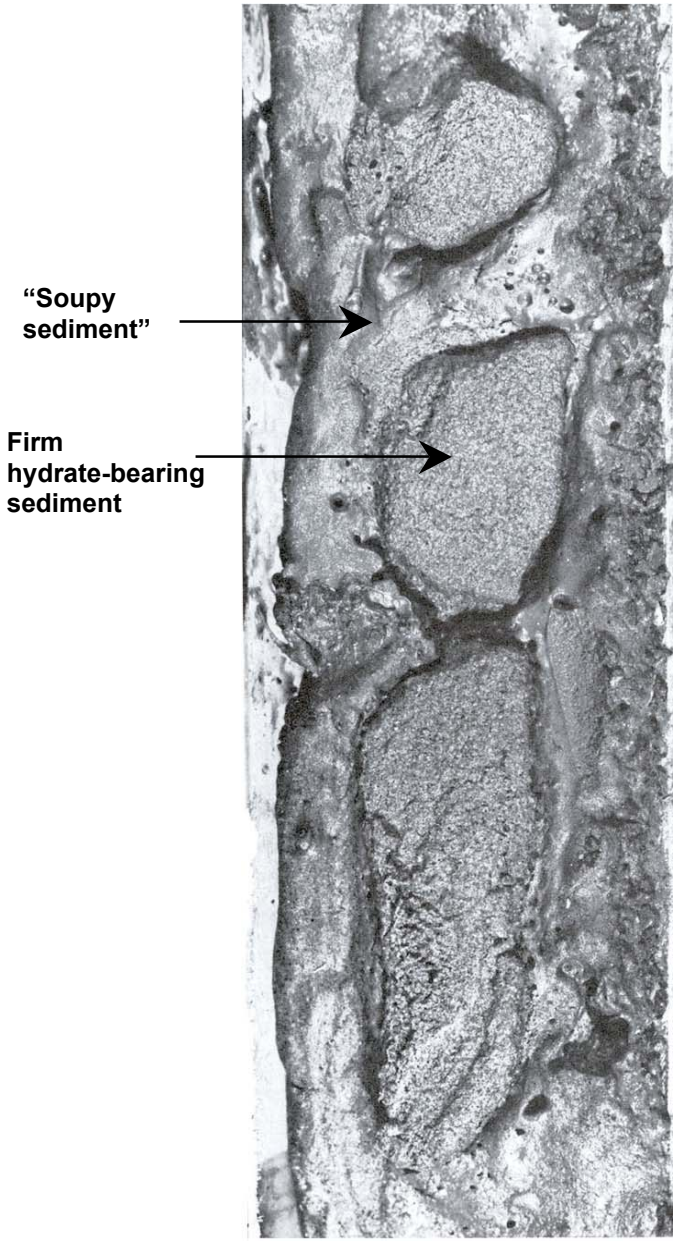

Figure 3 – Dissociating sample of a marine HBS core[14]. Note the firm appearance of the hydrate-bearing inner core, as opposed to the "soupy sediment" (soft mud of fluid consistency with evidence of bubbling gas) in the dissociating outer annulus (source: Deep Sea Drilling Program, Leg 67, courtesy of C.K Paull of the Monterey Bay Aquarium Research Institute).

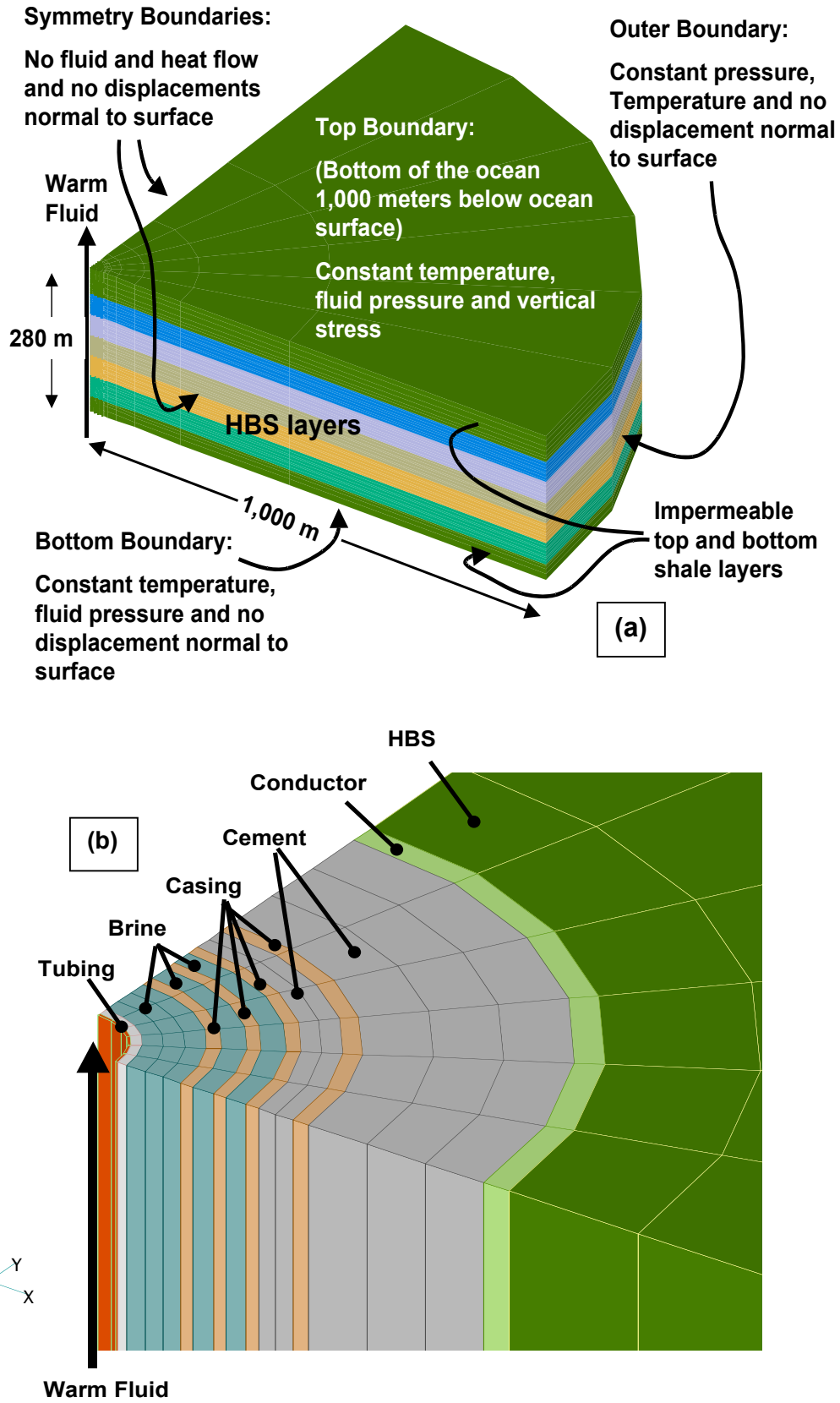

Figure 4 – Quarter-symmetric 3D model used in the analysis of Problem 1: (a) grid of the entire 3D domain, and (b) detail of the discretization of well assembly and its vicinity (see Table 4).

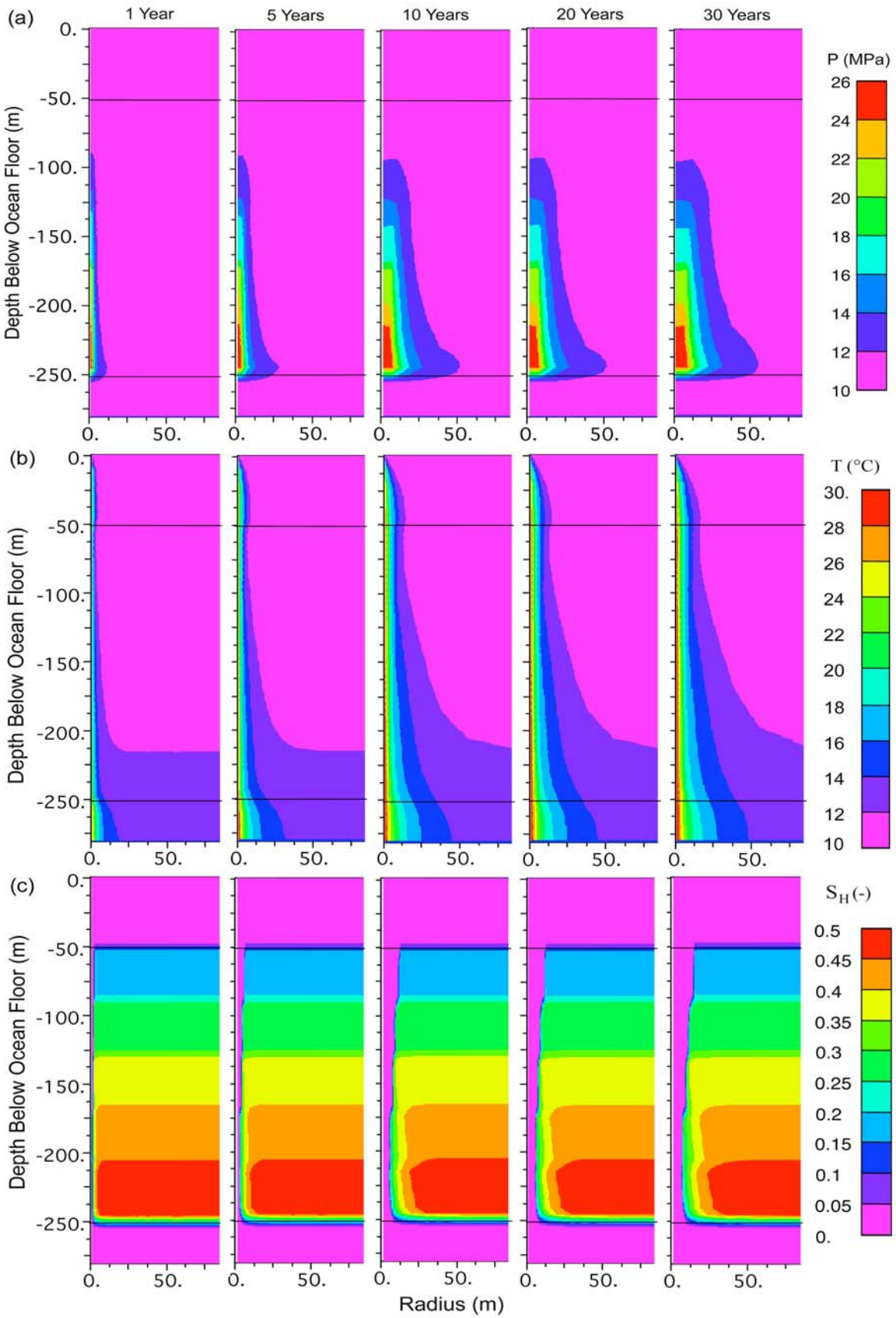

Figure 5 – Evolution of the spatial distributions of key variables in Problem 1 during 30 years of thermal loading: (a) pressure *P*, (b) temperature *T*, and (c) hydrate saturation S_H.

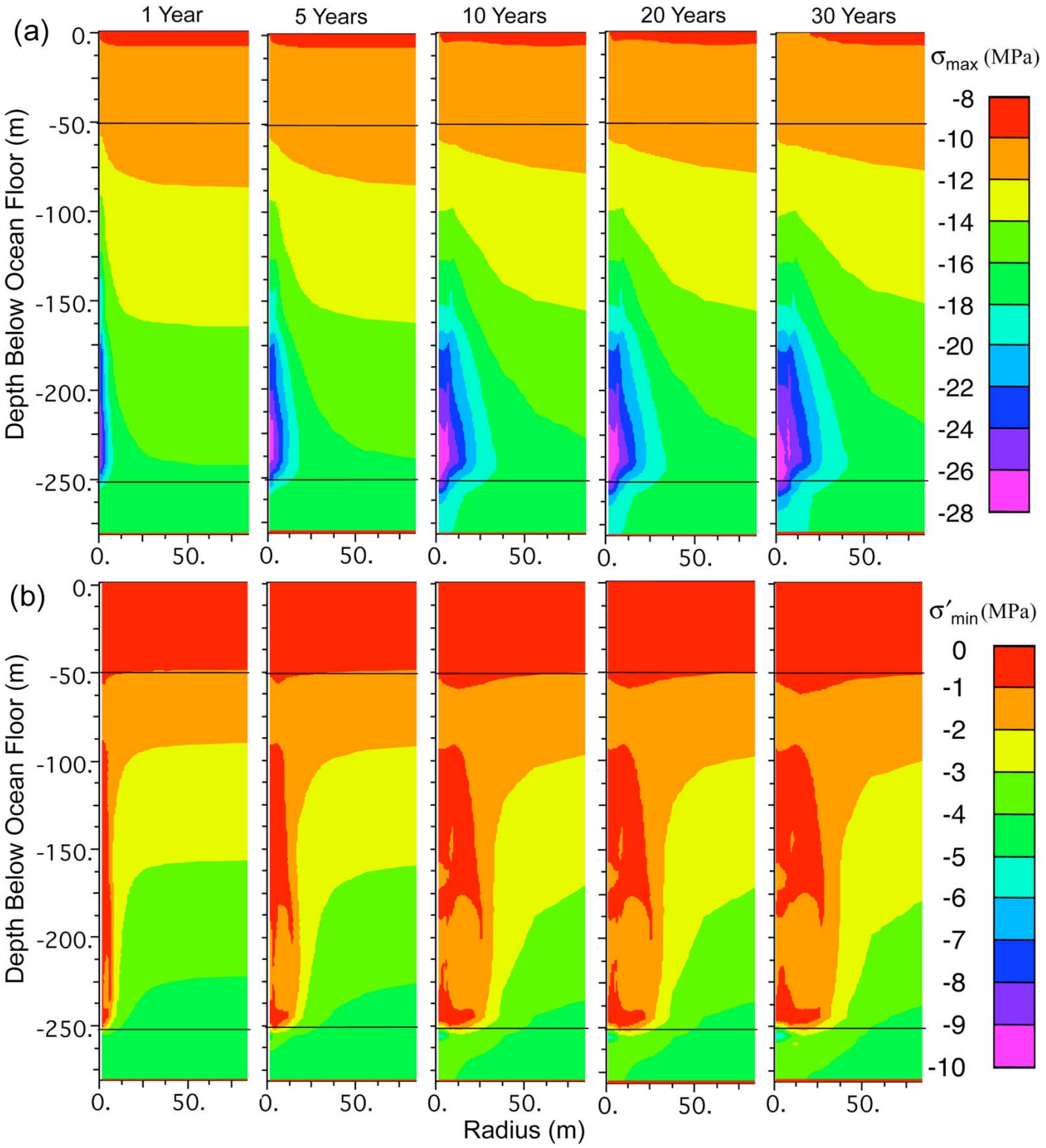

Figure 6 – Evolution of the spatial distributions (a) maximum compressive stress and (b) minimum compressive effective stress in Problem 1 during 30 years of thermal loading.

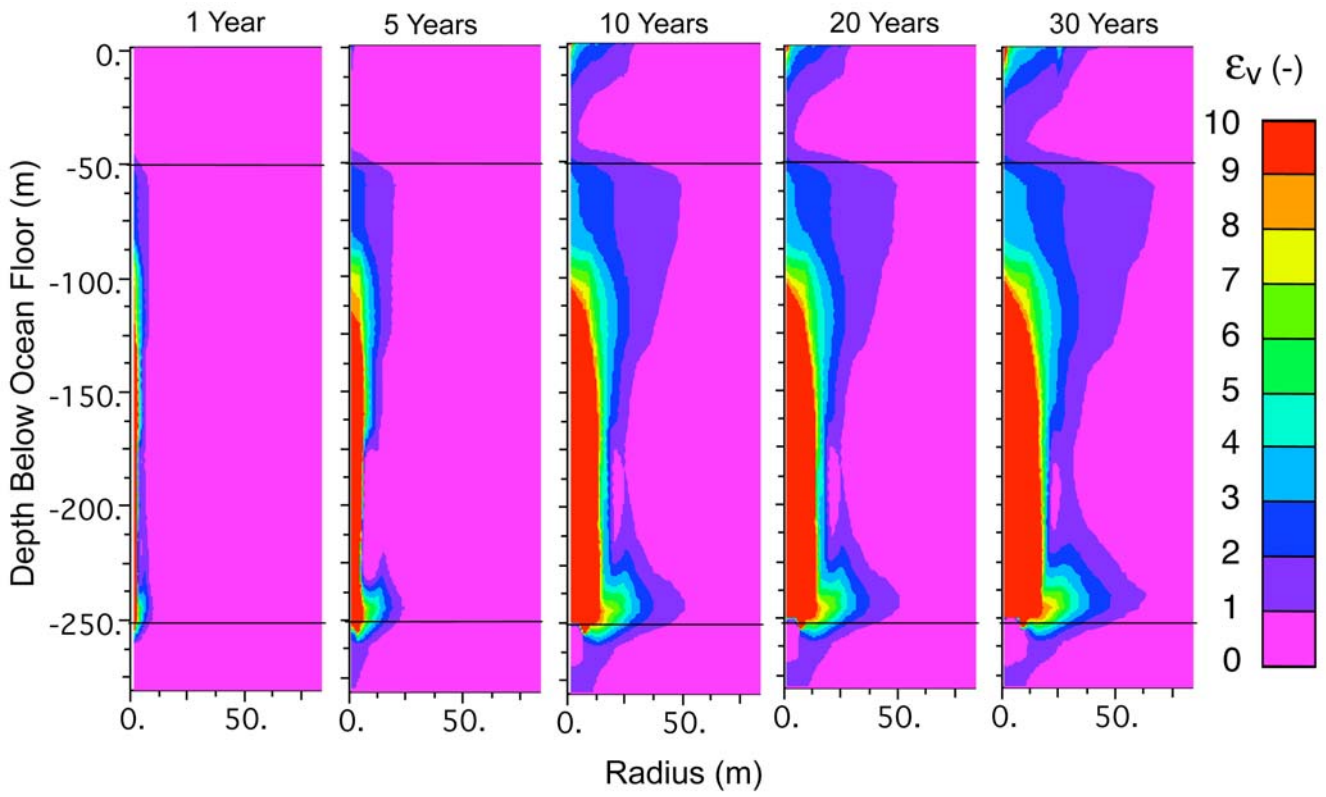

Figure 7 – Evolution of the spatial distribution of volumetric strain (indicating areas of significant plastic yield of the geological formations) in Problem 1 during 30 years of thermal loading. The mechanical properties of the HBS are those of the Toyoura sand[3].

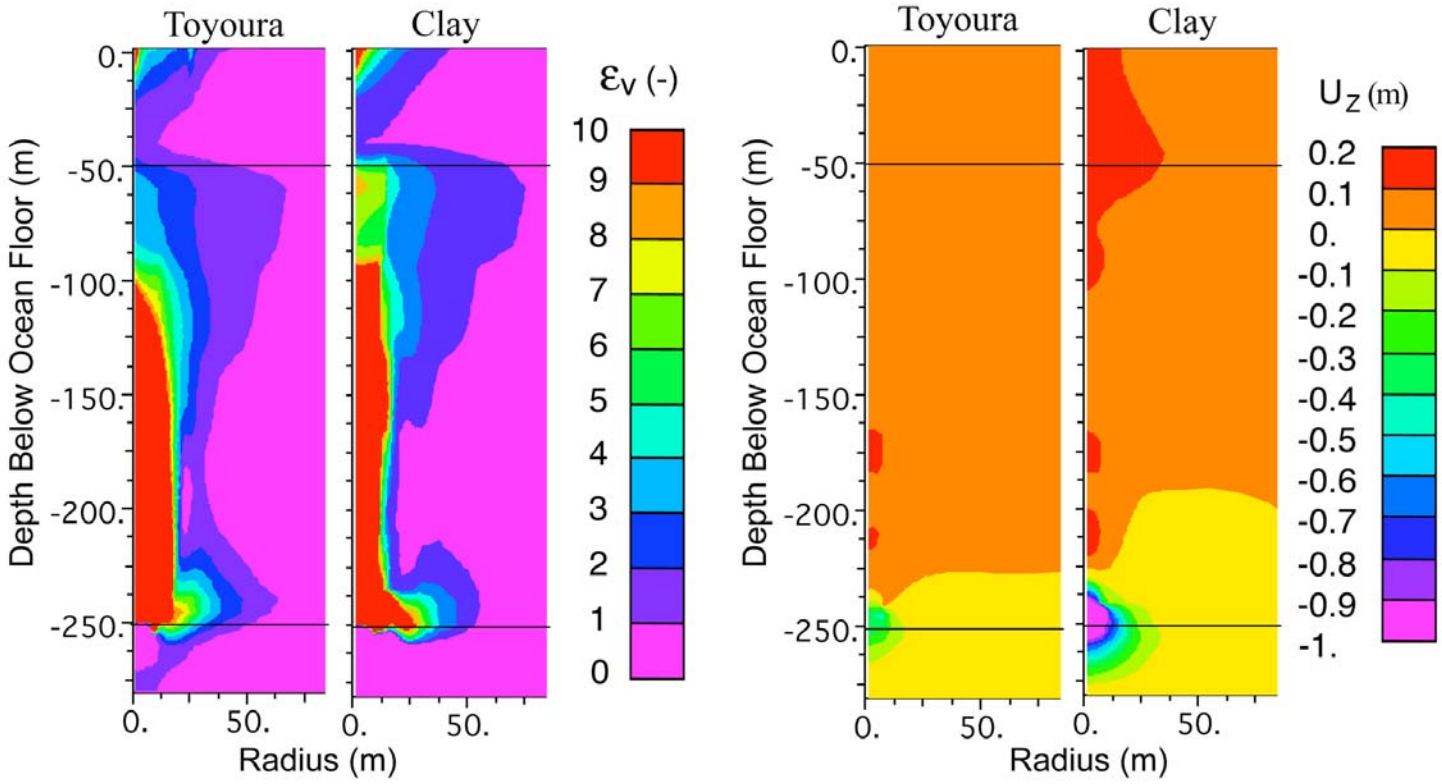

Figure 8 – Comparison of the system response in Problem 1 for two sets of geomechanical properties (Toyoura sand[3] and unconsolidated clay): spatial distributions of (a) volumetric strain (indicating areas of significant plastic) and (b) vertical displacement (subsidence or uplift) after 30 years of thermal loading.

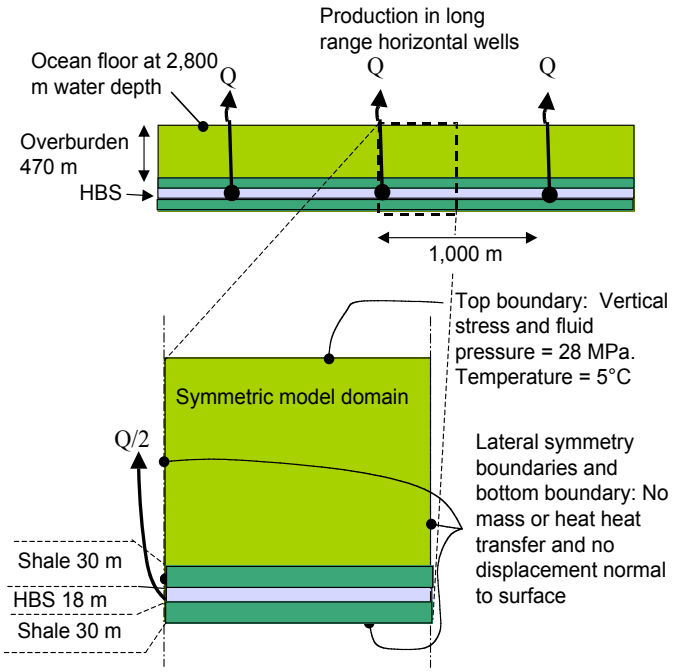

Figure 9 – Model geometry, boundary conditions, and domain description of Problem 2, investigating the geomechanical system response to gas production from a deep oceanic HBS using a horizontal weel.

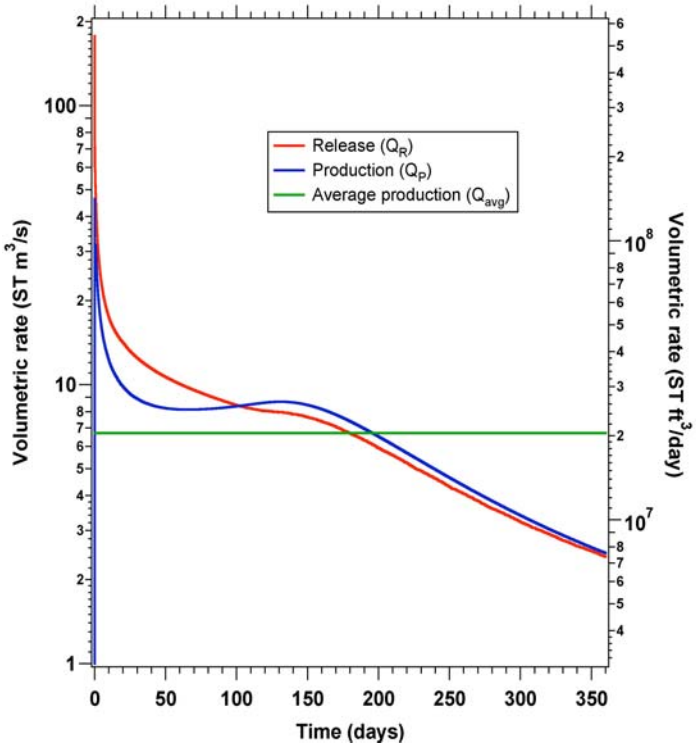

Figure 10 – Rates of hydrate-originating CH_4 release in the reservoir (Q_R) and CH_4 production at the well (Q_P) during production from the Class 3 oceanic hydrate deposit in Problem 2. The average production rate (Q_{avg}) over the simulation period (360 days) is also shown.

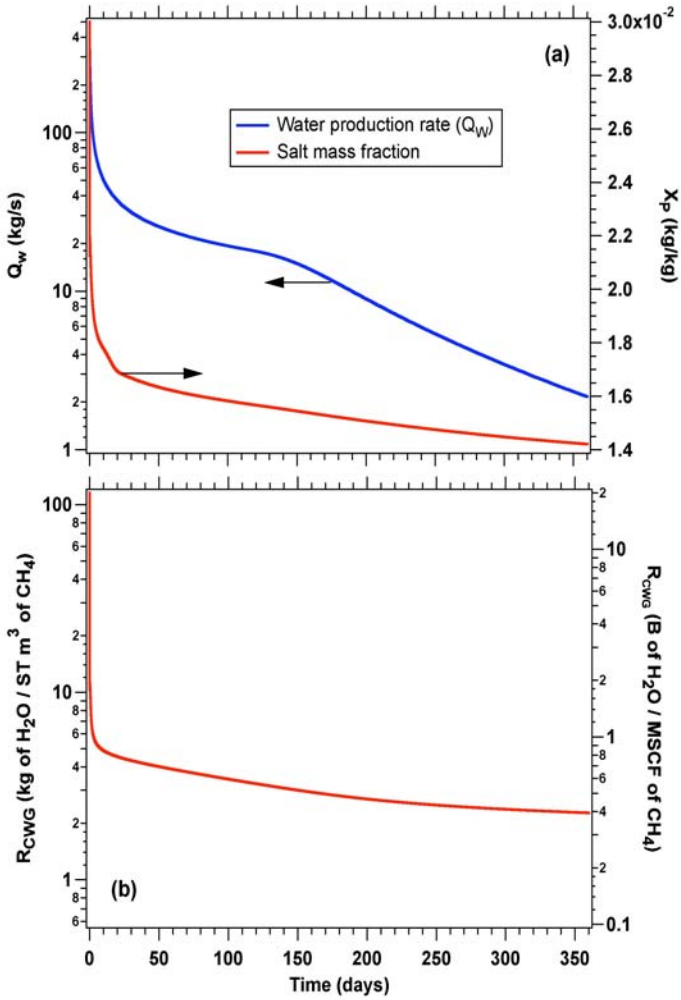

Figure 11 – Production from the Class 3 oceanic hydrate deposit in Problem 2: evolution of (a) the rate of H_2O production (Q_W) and salinity (X_P) of the produced water; (b) the cumulative water-to-gas ratio R_{CWG} during the production period.

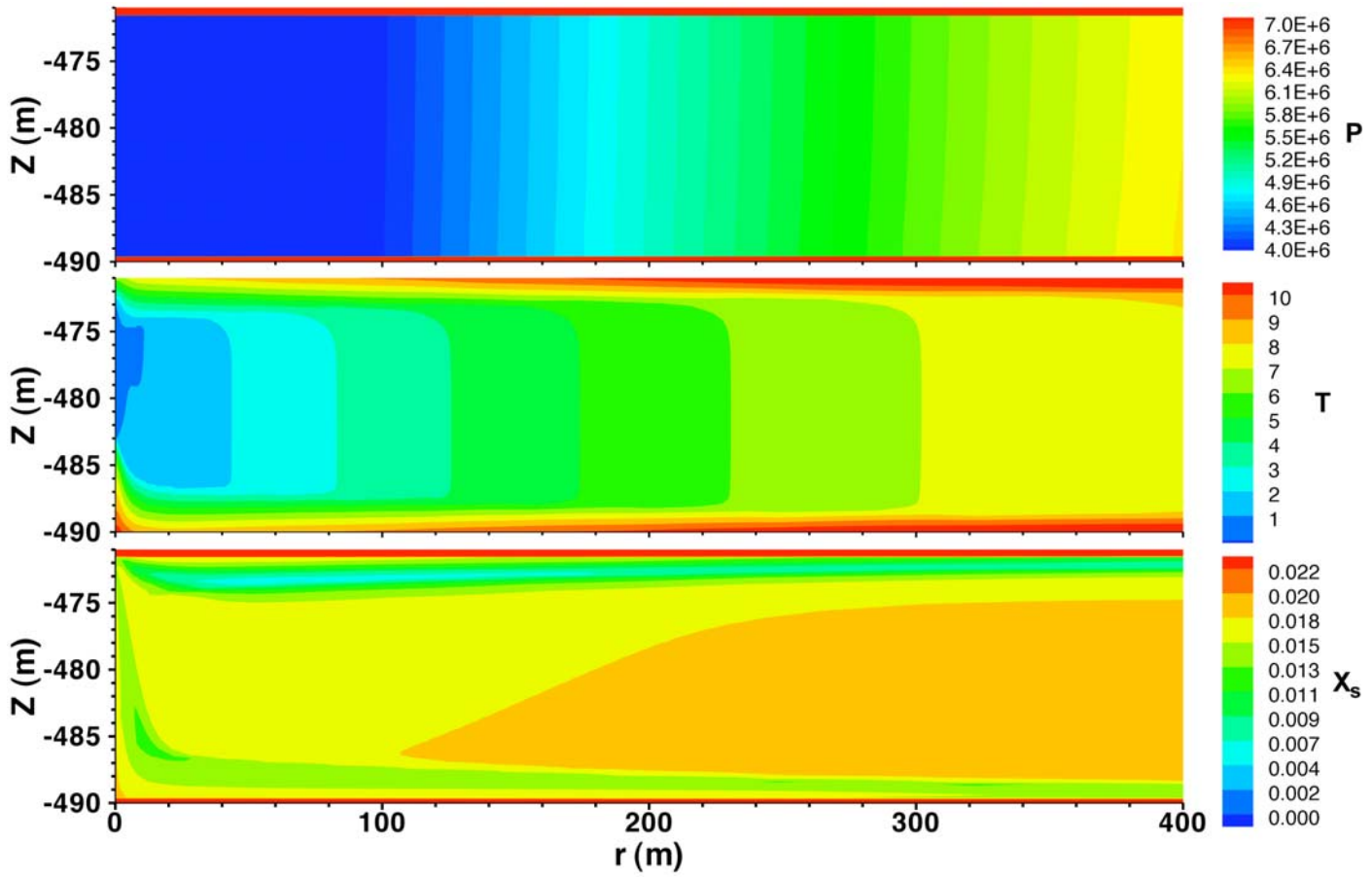

Figure 12 – Spatial distributions of key variables in Problem 2 at the end of 1 year of production using a horizontal well: (a) pressure *P*, (b) temperature *T*, and (c) salt mass fraction in the aqueous phase *X*.

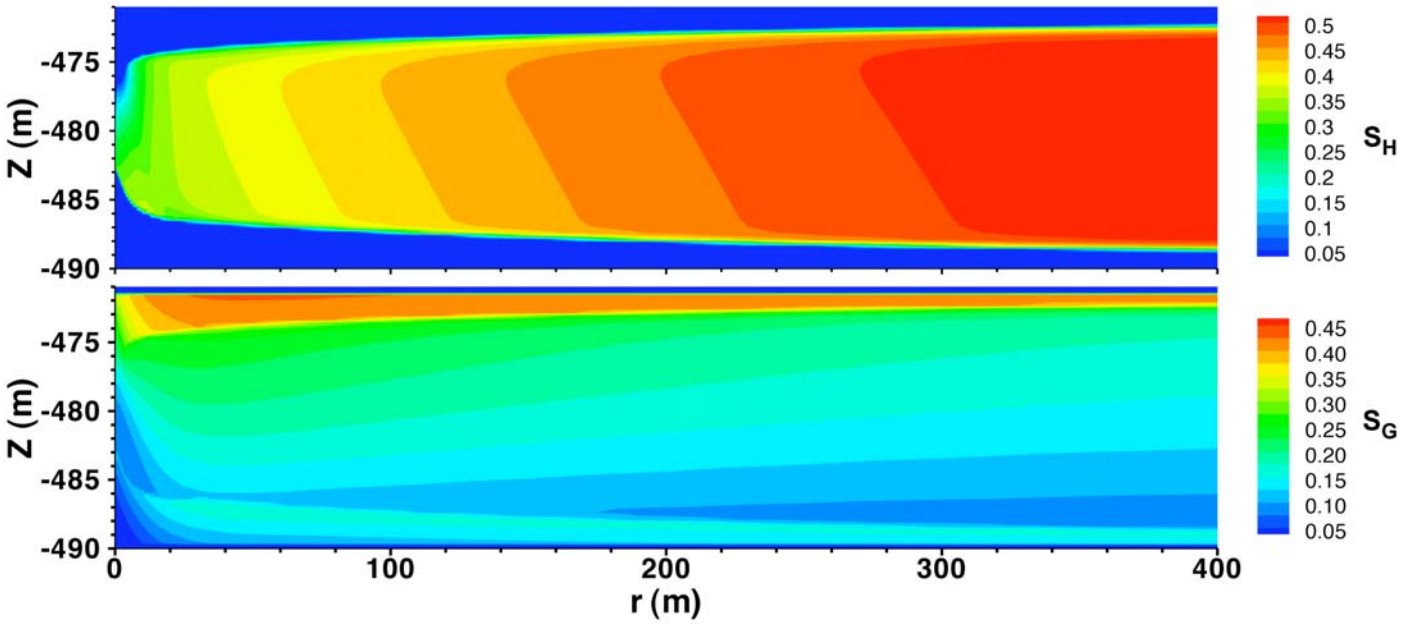

Figure 13 –Problem 2: Spatial distributions of (a) hydrate saturation S_H and (b) gas saturation S_G at the end of 1 year of production.

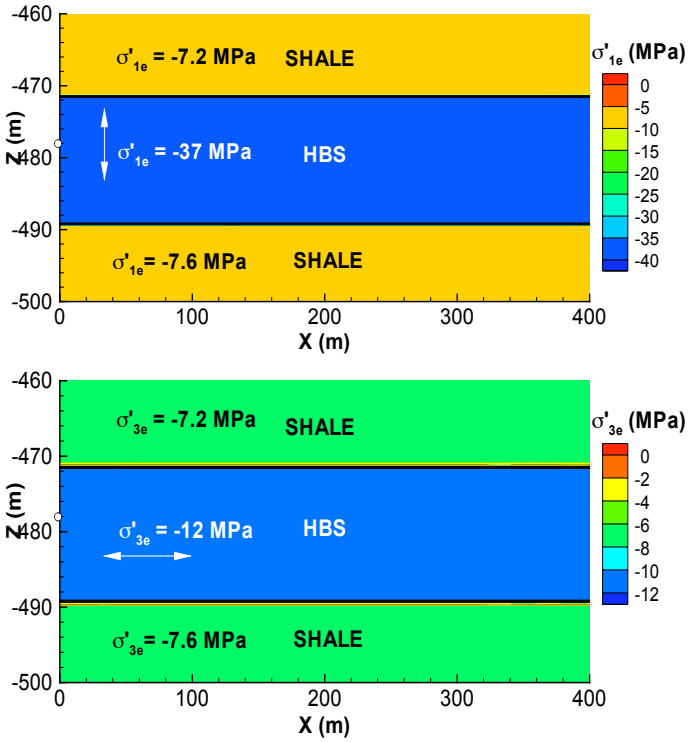

Figure 14 – Problem 2: spatial distributions of (a) maximum compressive effective stress and (b) minimum compressive effective stress after 1 year of gas production.

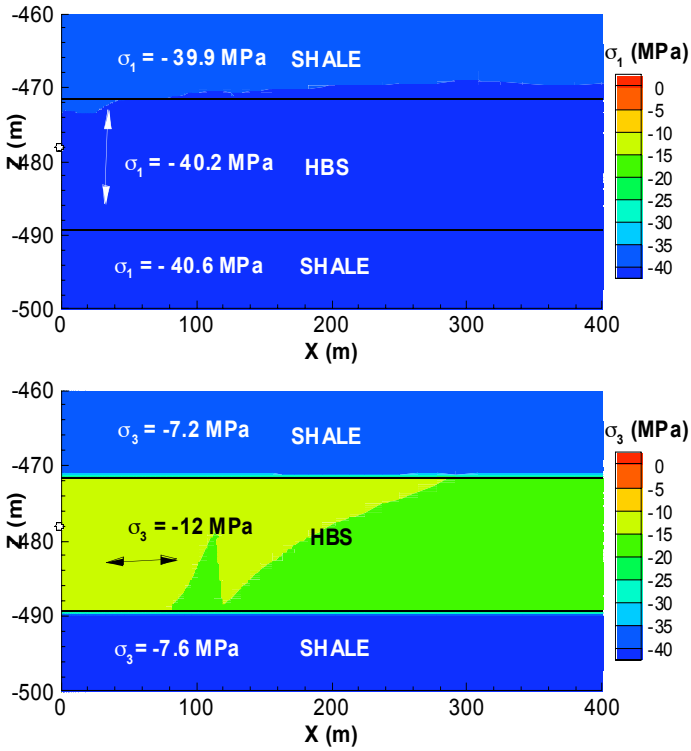

Figure 15 – Problem 2: spatial distributions of (a) maximum compressive stress and (b) minimum compressive stress after 1 year of gas production.

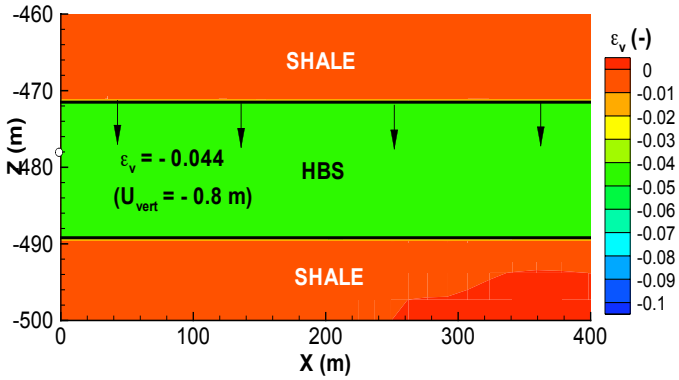

Figure 16 – Problem 2: Spatial distribution of the volumetric strain after 1 year of production. The vertical settlement (subsidence) U_{vert} is also indicated.